Journal of Materials and Electronic Devices 1 (2022) 7-16

The Photosensitive Properties of a new Photodiode consisting Thin Film CuAlMnNi Shape Memory Alloy Layer Contact

Oktay KARADUMAN[1], Canan Aksu CANBAY[1]*

[1]Department of Physics, Science Faculty, Firat University, Elazig, 23119, TURKEY

This work is based on fabrication and photoelectrical characterization of a new Schottky type metal-semiconductor photodiode including the thin film CuAlMnNi shape memory alloy layer that was coated as contact metal on n-Si wafer by thermal evaporation method. The photoelectrical current-voltage (I-V), current-time (I-t) and frequency based capacitance-voltage C-V signalization tests in darkness and varied artificially illuminated conditions were performed to find out the photoconductive, photovoltaic, photoresponsive and capacitive features. The forward bias I-V plots under dark and maximum illumination power were analysed by space charge current conduction analysis. The ideality factor and rectifying values of the photodiode was found increasing by the applied light. The photodiode with alloy film contact layer exhibited good photodiode figure of merits such as a maximum responsivity value of 46.5 mA/W, a remarkably high photosensitivity (%PS) value of 19330.29, and a huge specific detectivity value of 3.33×10^{10} Jones. These performance values imply that the new photodiode including thin film smart alloy layer can be useful in optoelectronic, sensor, and photodetector application fields.

Keywords: *Photodiodes, Thin film shape memory alloys, Schottky contact, Responsivity, Photosensitivity, Detectivity, Space charge limited current*

Submission Date: 11 February 2022
Acceptance Date: 02 May 2022

**Corresponding author: caksu@firat.edu.tr*

1. Introduction

Shape memory alloys (SMAs) as thin films have been recently used in fabrication of Schottky type metal-semiconductor (MS) photodiodes by coating these smart alloys with nano-dimensions onto semiconductor (silicon wafers) substrates [1–9]. However, the depth and number of such SMA-photodiode studies are inadequate and there is need to be done more in this infant aged research theme. For example the photodiode performans parameters of these photodiodes have not been studied enough yet, and use of more different alloy composition and production methods or other experimental and studying ways can be tried on.

Shape memory alloys are known as one of the most commercially used smart material group after piezoelectric materials. Their usage desirability and high future utilisation potentials in many application areas such as medical, actuator, aerospace, automotive, micro/nano electromechanical systems (M/NEMS) etc. [10–23] depend on their fascinating shape memory effect (SME), superelasticity (SE) and other properties like damping, strength or thermal and electrical properties they exhibit in bulk and miniature sizes.

In nano scales the properties of these alloys such as electrical, chemical, optical etc. are change like the properties of other materials do. SMA thin films can show shape memory effect behavior till the critical 20 nm of thickness [24]. The bulk and also micro and nano sized SMAs do this strain recovery as a sum of small microstructural alterations in their unit cells forced by internal stresses emerging from the temperature changes

that lead to a solid to solid phase transformation called as martensitic transformation. Such transformations occur between two solid phase of SMAs named as martensite (cold phase) and austenite (hot phase).

The electrical and thermal conductivity values of the famous and superior featured NiTi (or nitinol) SMAs [25–27] are much lower than copper based SMAs such as CuAlNi or CuAlMn [9,28–33]. Therfore the use of Cu-based SMAs as thin films in optoelectrical nanodevices like photodiodes makes sense. Besides, the Cu-based SMAs are much less expensive and more easily processable than NiTi ones.

Schottky type MS photodiodes are actually Schottky type MS diodes. They let current to flow in one voltage side and in the other side they only let a small saturation or leakage current. Therefore, these fast devices are mostly used as switching elements and transistors essentially in in modern electronic circuits. The photodiodes' ability to absorb light waves and transform into electrical signal paved the way for development of solar cells, photodetectors and varied kind of sensors and devices. Today, one part of the most important things about photodiodes is their performaces. Many efforts including fabricating similar kind photodiodes or other miscellenaous types of photodevices with many different materials and methods have been made to improve performance and functional usage of them until now [34–39].

In this research work, a new Schottky type metal-semiconductor photodiode with CuAlMnNi/n-Si/Al structure including the thin film CuAlMnNi shape memory alloy layer coated as top-contact metal on n-Si wafer was fabricated by thermal evaporation method. The photodiode characterization of obtained nanodevice was made by photoelectrical I-V, I-t and C-V tests under dark and light of different power intensities. Some important electrical diode parameters and photodiode figure of merits were determined.

2. Experimental Details

The used CuAlMnNi shape memory alloy with a composition of 69.65Cu-25.01Al-4.42Mn-0.92Ni (at.%) [40] was produced melting the pelletized mixture made of high purity (%99.99) metal element powders of Cu, Al, Mn and Ni in an arc melter chambered with argon plasma atmosphere. Then the obtained as-cast ingot alloy was underwent traditional post-homogenization and water-quenching treatments to install shape memory effect property. The thermal DSC, DTA and structural EDX and XRD measurements were performed to reveal the shape memory effect properties of the CuAlMnNi alloy. Full details on these production and characterization tests were given in the recent work [40] which is also a part of the same project including this work. Some results obtained from the characterization of the CuAlMnNi memory alloy were also given in this work briefly. To produce photodiode at first the n-Si wafer and CuAlMnNi and Al metal pieces were cleaned according to standard RCA cleaning procedure which consits of ultrasonic bathing in distilled water, acetone and ethyl alcohol for 5 min at every turn, then etching the n-Si in (1:10 ml) HF:H2O acid medium for 30 s, then washing by distilled water again and lastly drying with gas (nitrogen). The evaporation and coating of firstly Al metal piece on back face of n-Si for building ohmic contact then the SMA piece on front face of n-Si for building top Schottky contact were made by using a Nanovak thermal evaporation system. The evaporations were made when the chamber pressure reached to 2×10^{-6} Pa. After coating Al and before coating SMA the ohmic n-Si/Al structure was underwent in a post-annealing treatment at 570 °C for 5 min to improve surface contact between Al and n-Si layers. At room temperature, the SMA film also with 150 nm thickness was coated onto the front n-Si face placed behind of a mask with many small holes that each has an area (A) of 0.785×10^{-2} cm^2 which became to be the area of each CuAlMnNi top-diode-contact. The photoelectrical current-voltage (I-V), capacitance-voltage (C-V) and current-time (I-t) signalization tests on the manufactured CuAlMnNi/n-Si/Al photodiode were implemented under dark and varied increasing light power intensities by using FYM-7000 and -9000 model FYTRONIX Solar Simulator electronic characterization system equipments. A schematic looking of the produced SMA thin film layered photodiode can be seen in Figure 1.

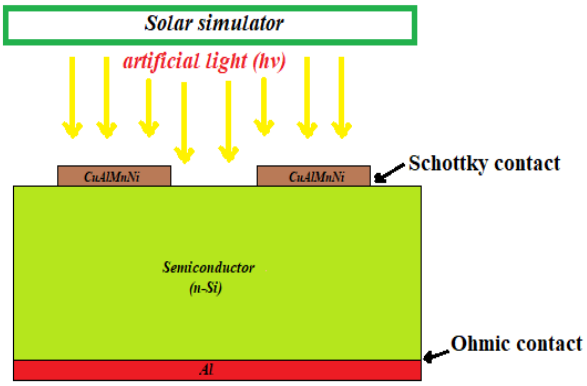

Fig.1. The schematic illustration of the produced CuAlMnNi/n-Si/Al photodiode.

.

3. Results and Discussions

The X-ray diffraction test (XRD) result made by using CuKα type X-waves for the CuAlMnNi shape memory alloy is presented in Figure 2. In this pattern showing many different small and shallow interwoven microcrystallographic phase peaks that make the alloy

highly polycrystal, the main diffraction peak belongs to the peak of γ1'(211) type martensite (M) phase which makes this phase the dominant martensite phase and the other observed martensite peaks are varied gamma type γ1'and beta type β1' martensite phases [40]. All of these martensite peaks mean that these phases constitute the underlying mechanism for the shape memory effect property of CuAlMnNi alloy. The precipitations appeared as the peaks of Cu-α(200) and a γ1(444)-Cu_9Al_4, plus the β1(200) and β1(331) were also seen as $L2_1$ austenite (A) phase peaks [40].

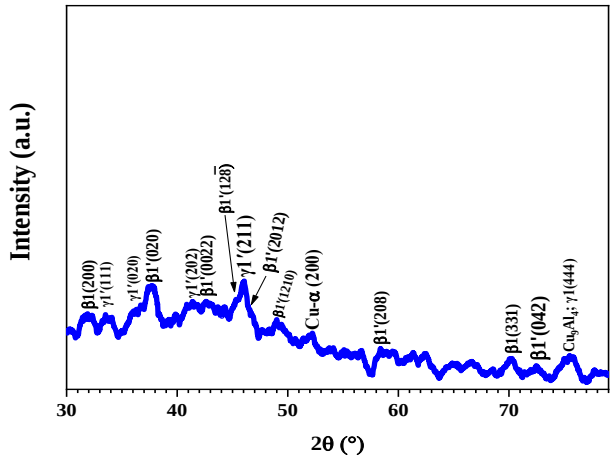

Fig.2. The XRD diffraction characteristic of the CuAlMnNi smart alloy.

According to the results of the differential scanning calorimetry (DSC) measurements (seen in Figure 3) taken at varied heating-cooling rates of 10-30 °C/min, there can be seen two types of peaks which indicate the solid to solid reversible martensitic transformations (the direct A→M or the reverse M→A transformations) occurred by the up and down changes of the temperature of CuAlMnNi alloy sample. Among these peaks, the downside large endothermic ones seen on the all heating process fragments of the each curve of heating-cooling rate indicate the martensite to austenite transformations, and the corresponding upside exothermic ones show the austenite to martensite phase transitions [11,26,28,30,40–46]. Therefore, the DSC results confirm the shape memory effect property of the alloy as a thermal response of it. By applying tangent differentiation method on these peaks via using the DSC software program, the characteristic thermodynamical parameters of peak (phase) start and finish temperatures (of A_s, A_f, M_s and M_f), hysteresis gap (A_s-M_f), equilibrium temperature (T_0) and the amounts of enthalpy (ΔH) and entropy (ΔS) differences occurred in these transformations determined directly and by computing [40] are given as average of the values at all heating-cooling rates in Table 1.

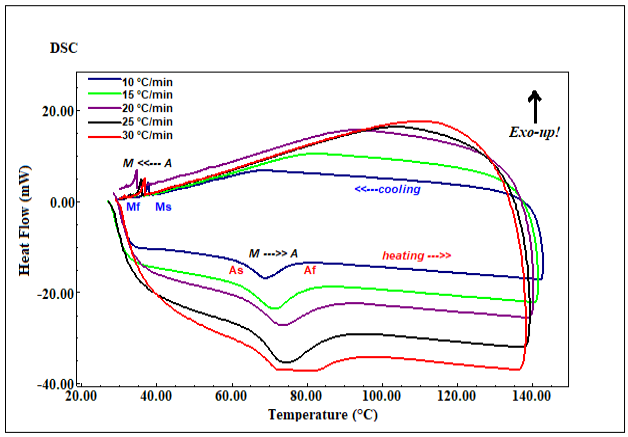

Fig.3. The characteristic DSC thermogram curves of the CuAlMnNi shape memory alloy.

Table-1: The determined average values of the thermodynamical martensitic phase transformation temperatures and other transformational parameters of the CuAlMnNi shape memory alloy.

Heating/cooling rate (°C/min)	A_s (°C)	A_f (°C)	A_{max} (°C)	M_s (°C)	M_f (°C)	A_s-M_f (°C)	T_0 (°C)	$\Delta H_{M\rightarrow A}$ (J/g)	$\Delta S_{M\rightarrow A}$ (J/g°C)
20 (Avg.)	64.20	82.11	72.16	36.37	35.38	28.82	59.24	7.965	0.1342

The result of another thermal analysis test, the differential thermal analysis (DTA) test, taken at single heating rate of 25 °C/min is presented in Figure 4. The sequent peaks start to be observed from far left to the far right on this DTA thermogram obtained by heating the CuAlMnNi alloy from room temperature to a high β-phase temperature (900 °C) are a chain of multiple phase transition reactions. These reactions are; β1'+γ1' (martensite) → $\beta1(L2_1$, austenite) → β2(semi-stable) → α+γ2 (hypoeutectoidal segregation) → eutectoid recomposing → β2(steady) → β(A2, irregular). These chain reactions are common high temperature behavior of the Cu-based SMAs [28–31,33,40–42,44,45,47–52].

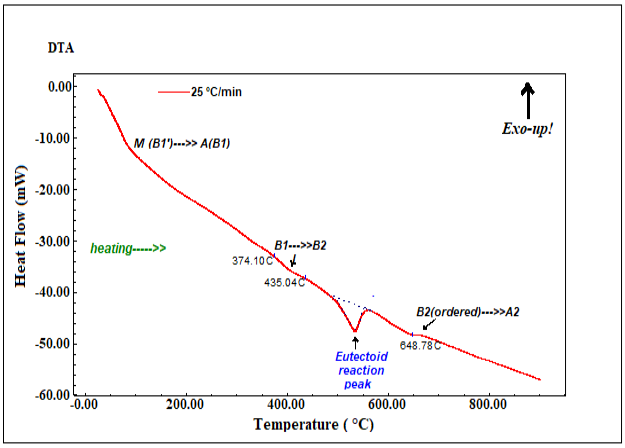

Fig.4. The DTA thermogram of the CuAlMnNi shape memory alloy.

The photoelectrical I-V test results as semi-log mode plots of the new CuAlMnNi/n-Si/Al photodiode obtained under the conditions of dark and different power intensities of imitated solar light illuminations are shown in Figure 5. As seen on these on these plots, except a small leakage current flowed in the reverse (negative) voltage bias region, the current was let to flow by the photodiode only in forward (positive) voltage bias region. So, the photodiode exhibited a current rectifying behavior. The values of the current rectification ratio (RR) parameter of the photodiode at ±5 V of voltage couple equal-in-absoulte were calculated by using RR(±V) = I(V)/I(-V) formula [9] and found as 19 for dark and 47.81 for 100 mW/cm^2 of light power intensity conditions, respectively. The increment of RR by the light effect means that the electrons extra-energized by light absorbation must have passed more deep traps than they did in the dark case. This will be confirmed by the results of current conduction mechanism analysis made on I-V plots that are given ahead.

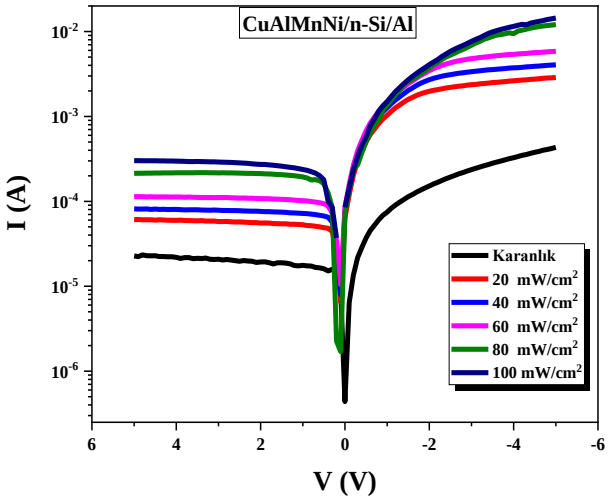

Fig.5. The characteristic semi-log *ln(I)-V* plots of the new CuAlMnNi/n-Si/Al SMA-photodiode obtained under dark and different light power intensity conditions.

The I-V plots also show the photoconductive photocurrent (electron-hole pair) generation in both reverse and forward bias regions as there some increments occurred by the light effect. And these increments seems to be proportional to the light power. So, it can be said that the fabricated new photodiode has photoconductive and photovoltaic features which comes from the photoelectric event. This event occur by excitation of the electrons in valance band by the absorbed incoming photons with sufficient energies larger than the band gap (E_g) of n-Si ($h\nu \geq E_g$).

Depending on the conventional thermionic emission (TE) theory, for a Schottky MS diode the relationship between current and voltage (for V>3kT/q condition) expressed by the equation [36,53] presented as below;

$$I = I_o exp\left(\frac{q(V-IR_S)}{nkT} - 1\right). \quad ..(1)$$

where; *k* stands for the Boltzmann constant, *V-IRs* refers to the voltage that drops across the metal-semiconductor junction, *q* is electron charge, *T* is temperature (T= 300 K), *n* is idealty factor (unitless) parameter of the diode, and I_0 is the saturation current in the reverse bias. By intercept of the linear segment of *ln(I)-V* plot in forward bias region the I_0 value is determined from the expression given as below;

$$I_0 = AA^*T^2 exp\left(-\frac{q\phi_b}{kT}\right) \quad (2)$$

where; ϕ_b is the Schottky barrier height (SBH) of the CuAlMnNi/n-Si/Al photodiode at zero voltage (V=0), *A** is Richardson constant (the theoretical value of *A** for n-Si is 112 A.cm^{-2} K^{-2}) [36,54], and *A* is the diode's area of the CuAlMnNi top contact (A=0.785×10^{-2} cm^2).The *n* ideality factor were calculated by substituting the slopes of the linear fragments of the *ln(I)-V* plots at forward bias in the formula below;

$$n = \frac{q}{kT}\left(\frac{dV}{d(ln\, I)}\right) \quad (3)$$

The ideality factor *n* of the CuAlMnNi/n-Si/Al photodiode was found as 22.7 in darkness condition and 13.9 in illuminated condition of 100 mW/cm^2 power intensity and these *n* values are higher than the ideal value (*n*=1). The deviations occurring in *n* values from the value of ideal one (1) are attributed to the impacts of interface states (traps), impurities and vacancies, non-uniform charge distribution in the interface, the non-homogenous SBH (ϕ_b) across the MS junction [35,53,55]. The value of the ϕ_b for the the new Schottky photodiode is computed by using the formula [53] as below;

$$\phi_b = \frac{kT}{q} ln\left(\frac{AA^*T^2}{I_0}\right) \quad .(4)$$

The ϕ_b of the CuAlMnNi/n-Si/Al photodiode was found as 0.559 eV 0.513 eV for dark and 100 mW/cm^2 of light power condition, respectively. The differences between the values of RR, ϕ_b, and *n* in the dark and light conditions occurred due to the carrier recombination-generation induced by the

illumination effect and the effect of interface trap states in the CuAlMnNi/n-Si interface [53,56].

The responsivity (R_{ph}) parameter is one of the significant figure of merit for a photodiode that shows the photodetecting performance of a photodedector, it shows how a photodevice absorbs and responds the light drops on it. R_{ph} is the ratio of the generated net photocurrent to the power of incoming light and is expressed by $R_{ph}=I_{ph}/P.A_{eff}$ formula [53]. Where I_{ph} refers to the net photocurrent ($I_{ph} = I_{light} - I_{dark}$), P is the incident light power intensity, and A_{eff} is the effectively illuminated area (6 mm^2) of the photodiode. For at -5 V of reverse bias, the net photocurrent R_{ph} responsivity values of the manufactured SMA-photodiode were found as 31.9 mA/W and 46.5 mA/W for the conditions of 20 mW/cm^2 and 100 mW/cm^2 of light power intensities, respectively. These responsivity values are found similar to those reported in some recent works [57,58]. Furthermore, here perhaps even higher responsivity values could be reached by applying larger light power intensities than 100 mW/cm^2 up to the the natural limit of the produced CuAlMnNi/n-Si/Al photodiode [53].

Another photodiode figure of merit parameter is the photosensitivity. It is defined as a measure of the photodiode's ability to absorb incoming light. The greater photosensitivity, the better light absorbtion. The unitless photosensitivity parameter (represented as PS or percent %PS) is calculated by a formula [53,55] expressed as $\%PS = [(I_{ph} - I_d)\times 100]/I_d$, where I_d is dark current. For at -5 V, the %PS values were found as 14447.2 and 19330.29 for the conditions of 20 mW/cm^2 and 100 mW/cm^2 of light power intensities, respectively. These values were found coherent with some previous reported ones [53,55,59].

Specific detectivity (D^*) is another important characteristic parameter for a photodiode which is expressed as a photodiode's capability of weak light signal detection [53]. For a photodiode (or photodetector) the larger detectivity value, the more sensitive detection of weak signals. Large detectivity photodiodes are relevant to be used in optoelectronic communication applications. In condition of shot-noise limit, the diode area (A_{eff}) normalized dedectivity D^* can be determined by using $D^*=R_{ph}/(2qI_d/A_{eff})^{1/2}$ formula [53,60], where q is electron charge. At reverse -5 V, the D^* value of the new photodiode was found as 3.33×10^{10} Jones and 3.33×10^{10} Jones for the conditions of 20 mW/cm^2 and 100 mW/cm^2 of light power intensities, respectively. These D^* values found for the novel CuAlMnNi/n-Si/Al photodiode here are found consistent with some D^* values [53,55,59,60] reported recently.

At forward voltage bias, the dominat current conduction mechanism analysis, also called as SCLC (space charge limited current) analysis [61–63], for the novel photodiode was made by over the slope (m) values found by taking linear fitting on the double-log mode *ln(I)-ln(V)* plots of the dark and maximum power (100 mW/cm^2) of light conditions which are given in Figure 6. According to the determined m slope values of the these two plots, the dark forward bias *ln(I)-ln(V)* plot keeps a single $m\approx1$ slope value throughout the all forward bias voltage region and this slope value of 1 indicates that the dominant current transport mechanism for dark condition is fully an ohmic conduction. As to the plot for the 100 mW/cm^2 of light condition, the slope changed multiple times due to the light effect. So, at first near the zero voltage on the far left of this plot (the I.Region) the 0.69 slope value is lower than unity (1) that means a current conduction based on electron tunneling is the dominant conduction mechanism in this linear plot fragment (because the electrons have insufficient energies in this low voltage region to pass across the barrier height so they pass across the Schottky interface by tunneling). Then the slope becomes nearly 1 (0.99) in II.Region which means that the ohmic conduction mechanism (defined by linear $I \propto V$ power law relationship) is the dominant mechanism here caused by the movement of the mobile electrons in conduction band or similarly holes in valence band [63] and electrons also make tunneling between the interface states. In III.Region the slope was evolved to the values around ~1.5 which indicates a trap filling limited SCLC (space charge limited current) mechanism ($I\propto V^{1.5}$) is the dominant current conduction mechanism in this region [61–63], that was caused by the energising electrons by the effect of applied illumination. So, by this means, the electrons with more energies passed over the deep bulk traps potential barriers and thus they contributed to the total current.

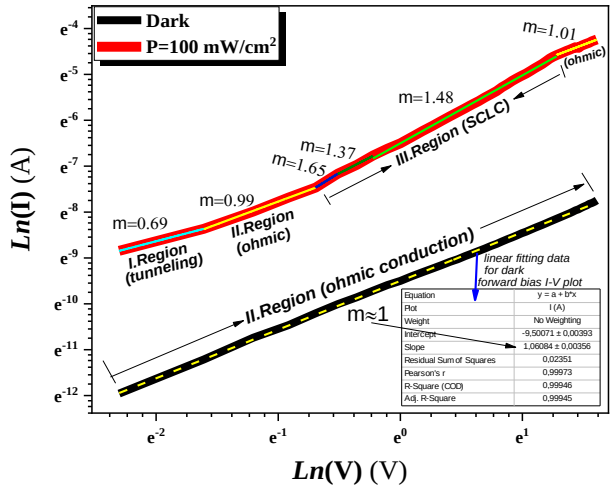

Fig.6. The double-log mode *ln(I)-ln(V)* plots under the dark and maximum power (100 mW/cm^2) of light conditions for the fabricated CuAlMnNi/n-Si/Al photodiode. The ohmic current conduction mechanism in dark condition evolves to trap filling limited SCLC mechanism in illuminated condition.

The time-dependent dynamic current-time I-t test (TPC test) result is presented in Figure 7. By this test the charge carriers generated as photocurrent by the effect of light was analyzed. As seen, a nearly steady-state photocurrent proportional to the applied light power is generated whenever the light turned on by the solar simulator. When the light is turned off at the end of each light applied processes the current level rapidly goes down to the ground

level. This result shows that the fabricated photodiode has a photovoltaic property that makes it to convert the light energy into electric energy.

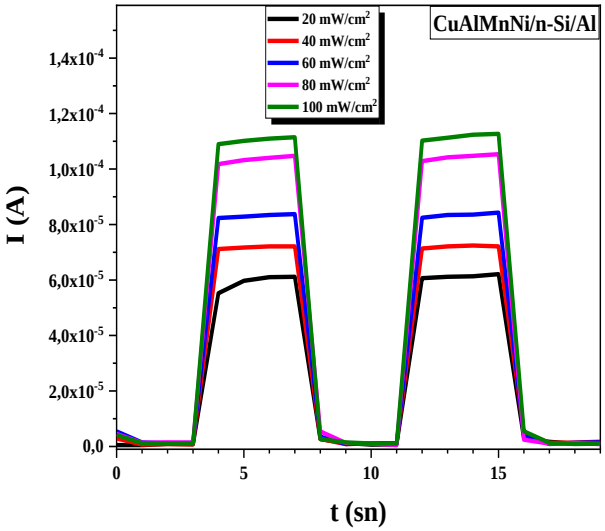

Fig.7. The dynamic *I-t* current-time (TPC) curves of the CuAlMnNi/n-Si/Al photodiode.

The results of the capacitance-voltage (C-V) measurements taken by different increasing steps of frequencies in the range between 10 kHz and 1 Mhz are given in Figure 8. While no any capacitance was observed at forward voltage bias on right side (this voltage region is negative due to the use of opposite probe in this measurements), there is a capacitance in the reverse bias decreasing by the increase of the applied frequency. This happens because the electrons cannot follow the ac current at high frequencies [9].

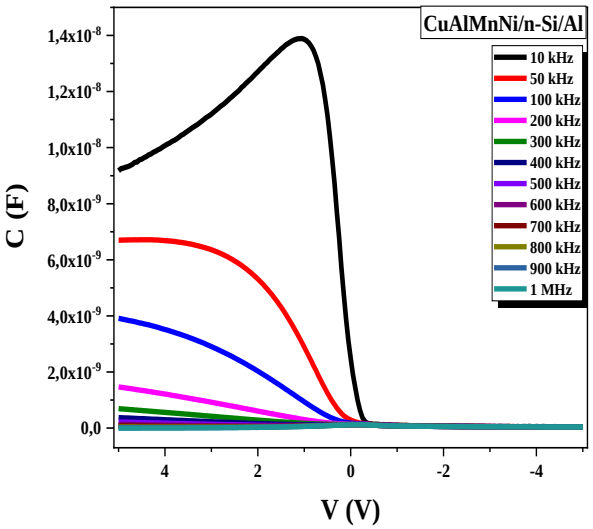

Fig.8. The capacitance-voltage curves of the novel CuAlMnNi/n-Si/Al photodiode obtained at different frequencies.

Some electrical contact parameters of the new photodiode can be found by drawing the inverse squared capacitance-voltage (C^{-2}-V) curves. These curves are given in Figure 9. At the reverse bias of (negative voltage) region on the left side of these curves by using the linear fitting value obtained from the graphic at 1 MHz the values of the non-compensated ionized donor atoms concentration (N_D) and diffusion potential (V_d) can be found. to the *x*-axis (voltage) The concentration of donor atoms, N_D can be calculated by the formula [9].as following below;

$$N_D = \frac{2}{q\varepsilon_0\varepsilon_s A^2}\left[\frac{d(C^{-2})}{dV}\right]^{-1} \quad (6)$$

where, V is applied potential, C is capacitance of depletion layer, q is electron charge, ε_0 is permittivity of space, ε_s is permittivity of the semiconductor and equal to 11.8 for n-Si, and A is diode area. By substituting the slope value of the C^{-2}-V plot at 1 MHz instead of $[d(C^{-2})/d(V)]^{-1}$ term in Eq.6 the N_d value was found as 1.65×10^{15} cm^{-3}. By linear extrapolation of the C^{-2}-V plot to the *x*-axis the V_d was found as 0.424 V. Furthermore, apart from the I-V method also the Schottky barrier height (ϕ_b) parameter can be calculated from the C^{-2}-V method by using the formula following as below;

$$\phi_b = \frac{V_d}{n} + \frac{kT}{q} ln\left(\frac{N_C}{N_D}\right) \quad (7)$$

where; N_C stands for the effective density of states in the conduction band of n-Si (N_C = 2.8 × 10^{19} cm^{-3}). Thus, the value of ϕ_b was found as 0.271 eV and this value was found lower than that value of 0.559 eV found by *I-V* method above. The reason for this may be that no any insulator interlayer was placed in between CuAlMnNi and n-Si layers which would increase the capacitance of the fabricated photodiode. The effective Fermi energy (E_F) was also calculated as 0.252 eV by using $E_F = \phi_b - (V_d/n)$ relation.

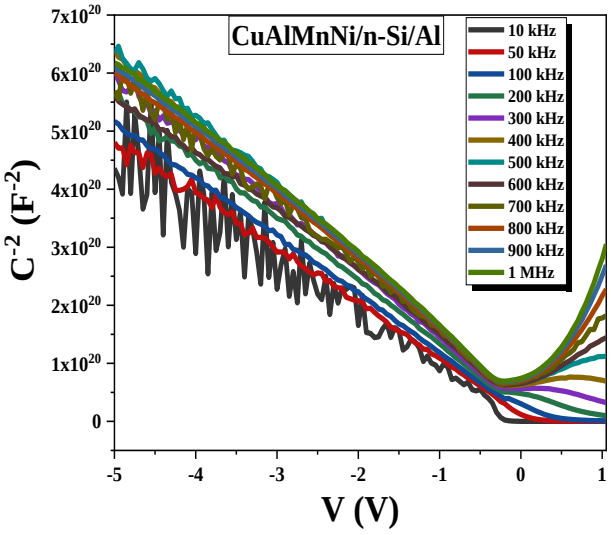

Fig.9. The inverse squared capacitance-voltage (C^{-2}-V) curves of the new CuAlMnNi/n-Si/Al photodiode obtained at different frequencies.

4. Conclusions

In this work, the novel MS Schottky type CuAlMnNi/n-Si/Al photodiode consisting nanofilm layer of CuAlMnNi shape memory alloy coated onto n-Si wafer was successfully produced by using thermal evaporation method. The used CuAlMnNi alloy has a highly polycrystalline structure consisting of martensite phases. By making photo-electrical I-V, I-t and C-V tests the new photodiode was characterized and some important electrical diode and photodiode parameters were determined. The high ideality factor deviated from unity was caused mainly from the presence of impurities, vacancies, interface states, non-uniform distribution of the interface charges and barrier inhomogeneity across the CuAlMnNi/n-Si contact. The ohmic current conduction mechanism was determined as the dominant conduction mechanism at forward bias and under dark condition, but by the electron energising effect of applied light under maximum light power intensity condition the trap filling SCLC current conduction mechanism ($I \propto V^{1.5}$) became the dominant conduction mechanism. The device exhibited good photovoltaic and photoconductive characteristics. It performed also good photodiode figure of merits such as a high responsivity, photosensitivity (%PS) and specific detectivity maxima values of 46.5 A/W, 19330.29 and 3.33×10^{10} Jones, respectively. The electrons were seen not able to follow the applied ac signal at high frequencies observed by C-V tests. All of the obtained results showed that the new shape memory alloy thin film layered photodiode can be useful in optoelectronic sensor or photodedector related applications.

Acknowledgements

This research work is a part of Ph.D. thesis works of Oktay KARADUMAN supervised by Prof. Dr. Canan Aksu CANBAY at Firat University, Faculty of Science, Department of Physics and was financially supported by FÜBAP, Project No: FF.21.14.

References

[1] C.A. Canbay, A. Tataroğlu, W.A. Farooq, A. Dere, A. Karabulut, M. Atif, A. Hanif, CuAlMnV shape memory alloy thin film based photosensitive diode, Materials Science in Semiconductor Processing. 107 (2020) 104858. https://doi.org/10.1016/J.MSSP.2019.104858.

[2] C.A. Canbay, A. Tataroglu, A. Dere, A. Al-Ghamdi, F. Yakuphanoglu, A new shape memory alloy film/p-Si solar light four quadrant detector for solar tracking applications, Journal of Alloys and Compounds. 688 (2016) 762–768. https://doi.org/10.1016/J.JALLCOM.2016.07.087.

[3] E. Aldırmaz, A. Tataroğlu, A. Dere, M. Güler, E. Güler, A. Karabulut, F. Yakuphanoglu, Cu-Al-Mn shape memory alloy based Schottky diode formed on Si, Physica B: Condensed Matter. 560 (2019) 261–266. https://doi.org/10.1016/j.physb.2018.12.024.

[4] E. Aldırmaz, A. Tataroğlu, A. Dere, M. Güler, E. Güler, A. Karabulut, F. Yakuphanoglu, Cu-Al-Mn shape memory alloy based Schottky diode formed on Si, Physica B: Condensed Matter. 560 (2019) 261–266. https://doi.org/10.1016/J.PHYSB.2018.12.024.

[5] C. Aksu Canbay, A. Dere, K. Mensah-Darkwa, A. Al-Ghamdi, Z. Karagoz Genç, R.K. Gupta, F. Yakuphanoglu, New type of Schottky diode-based Cu–Al–Mn–Cr shape memory material films, Applied Physics A: Materials Science and Processing. 122 (2016). https://doi.org/10.1007/s00339-016-0208-3.

[6] C.A. Canbay, A. Tataroğlu, A. Dere, A.G. Al-Sehemi, A. Karabulut, A.A. Al-Ghamdi, F. Yakuphanoglu, Electrical, kinetic and photoelectrical properties of CuAlMnMg shape memory alloy/n-Si Schottky diode, Journal of Alloys and Compounds. 888 (2021) 161600. https://doi.org/10.1016/J.JALLCOM.2021.161600.

[7] C. Aksu Canbay, A. Dere, K. Mensah-Darkwa, A. Al-Ghamdi, Z. Karagoz Genç, R.K. Gupta, F. Yakuphanoglu, New type of Schottky diode-based Cu–Al–Mn–Cr shape memory material films, Applied Physics A: Materials Science and Processing. 122 (2016). https://doi.org/10.1007/s00339-016-0208-3.

[8] E. Aldirmaz, M. Guler, E. Guler, A. Dere, A. Tataroğlu, A.G. Al-Sehemi, A.A. Al-Ghamdi, F. Yakuphanoglu, A shape memory alloy based on photodiode for optoelectronic applications, Journal of Alloys and Compounds. 743 (2018) 227–233. https://doi.org/10.1016/J.JALLCOM.2018.01.380.

[9] C.A. Canbay, O. Karaduman, The photo response properties of shape memory alloy thin film based photodiode, Journal of Molecular Structure. 1235 (2021). https://doi.org/10.1016/j.molstruc.2021.130263.

[10] J. Mohd Jani, M. Leary, A. Subic, M.A. Gibson, A review of shape memory alloy research, applications and opportunities, Materials and Design. 56 (2014) 1078–1113. https://doi.org/10.1016/j.matdes.2013.11.084.

[11] K. Otsuka, C.M. Wayman, Shape memory materials, Cambridge University Press, 1999.

[12] P. Krulevitch, A.P. Lee, P.B. Ramsey, J.C. Trevino, J. Hamilton, M. Allen, Thin film shape memory alloy microactuators, 1996. https://doi.org/10.1109/84.546407.

[13] Y.Q. Fu, J.K. Luo, A.J. Flewitt, W.M. Huang, S. Zhang, H.J. Du, W.I. Milne, Thin film shape memory alloys and microactuators, Int. J. Computational Materials Science and Surface Engineering. 2 (2009) 208–226. https://doi.org/10.1504/IJCMSSE.2009.027483.

[14] Y.Q. Fu, J.K. Luo, W.M. Huang, A.J. Flewitt, W.I. Milne, Thin film shape memory alloys for optical sensing applications, Journal of Physics: Conference Series. 76 (2007). https://doi.org/10.1088/1742-6596/76/1/012032.

[15] Y. Fu, H. Du, W. Huang, S. Zhang, M. Hu, TiNi-based thin films in MEMS applications: A review,

Sensors and Actuators, A: Physical. 112 (2004) 395–408. https://doi.org/10.1016/j.sna.2004.02.019.

[16] Y. Motemani, P.J.S. Buenconsejo, A. Ludwig, Recent Developments in High-Temperature Shape Memory Thin Films, Shape Memory and Superelasticity. 1 (2015). https://doi.org/10.1007/s40830-015-0041-0.

[17] N. Choudhary, D. Kaur, Shape memory alloy thin films and heterostructures for MEMS applications: A review, Sensors and Actuators, A: Physical. 242 (2016) 162–181. https://doi.org/10.1016/j.sna.2016.02.026.

[18] D.J. Fernandes, R. v. Peres, A.M. Mendes, C.N. Elias, Understanding the Shape-Memory Alloys Used in Orthodontics, ISRN Dentistry. 2011 (2011) 1–6. https://doi.org/10.5402/2011/132408.

[19] Z. He, K.R. Gall, L.C. Brinson, Use of Electrical Resistance Testing to Redefine the Transformation Kinetics and Phase Diagram for Shape-Memory Alloys, n.d.

[20] S. Yang, F. Zhang, J. Wu, Y. Lu, Z. Shi, C. Wang, X. Liu, Superelasticity and shape memory effect in Cu–Al–Mn–V shape memory alloys, Materials & Design. 115 (2017). https://doi.org/10.1016/j.matdes.2016.11.035.

[21] A. Concilio, V. Antonucci, F. Auricchio, L. Lecce, E. (Eds.). Sacco, Shape Memory Alloy Engineering, 2nd ed., Elsevier, 2021. https://doi.org/10.1016/C2018-0-02430-5.

[22] J. Ma, I. Karaman, R.D. Noebe, High temperature shape memory alloys, International Materials Reviews. 55 (2010) 257–315. https://doi.org/10.1179/095066010X12646898728363.

[23] A. Rao, A.R. Srinivasa, J.N. Reddy, Introduction to shape memory alloys, SpringerBriefs in Applied Sciences and Technology. (2015) 1–31. https://doi.org/10.1007/978-3-319-03188-0_1.

[24] P. Lega, A. Kartsev, I. Nedospasov, S. Lv, X. Lv, N. Tabachkova, A. Irzhak, A. Orlov, V. Koledovy, Blocking of martensitic transition at the nano-scale in the Ti2NiCu wedge, (2020). https://doi.org/10.1103/PhysRevB.101.214111.

[25] J.W. Mwangi, L.T. Nguyen, V.D. Bui, T. Berger, H. Zeidler, A. Schubert, Nitinol manufacturing and micromachining: A review of processes and their suitability in processing medical-grade nitinol, Journal of Manufacturing Processes. 38 (2019). https://doi.org/10.1016/j.jmapro.2019.01.003.

[26] C.A. Canbay, O. Karaduman, İ. Özkul, Lagging temperature problem in DTA/DSC measurement on investigation of NiTi SMA, Journal of Materials Science: Materials in Electronics. 31 (2020). https://doi.org/10.1007/s10854-020-03881-y.

[27] G.B. Kauffman, The Story of Nitinol: The Serendipitous Discovery of the Memory Metal and Its Applications, The Chemical Educator. 2 (1997) 1–21. https://doi.org/10.1007/s00897970111a.

[28] O. Karaduman, C.A. Canbay, Investigation of CuAlNi Shape Memory Alloy Doped with Graphene, Journal of Materials and Electronic Devices. 3 (2021) 8–14. http://www.dergi-fytronix.com/index.php/jmed/article/view/145.

[29] O. Karaduman, İ. Özkul, C.A. Canbay, Shape memory effect characterization of a ternary CuAlNi high temperature SMA ribbons produced by melt spinning method, Advanced Engineering Science. 1 (2021) 26–33. http://publish.mersin.edu.tr/index.php/ades.

[30] C. Canbay, O., Karaduman, P.A. Ibrahim, I. Ozkul, Thermostructural shape memory effect observations of ductile Cu-Al-Mn smart alloy, Advances in Materials Research. 10 (2021) 45–56. https://doi.org/https://doi.org/10.12989/amr.2021.10.1.045.

[31] O. Karaduman, C. Aksu Canbay, N. Ünlü, S. Özkul, Analysis of a newly composed Cu-Al-Mn SMA showing acute SME characteristics, in: AIP Conference Proceedings, American Institute of Physics Inc., 2019. https://doi.org/10.1063/1.5135437.

[32] O., Karaduman, C., Aksu Canbay, İ., Özkul, S., Aziz Baiz, N. Ünlü, Production and Characterization of Ternary Heusler Shape Memory Alloy with A New Composition, JOURNAL OF MATERIALS AND ELECTRONIC DEVICES. 1 (2018) 9–16. http://www.dergi-fytronix.com/index.php/jmed/article/view/24 (accessed October 14, 2021).

[33] R. Dasgupta, A look into Cu-based shape memory alloys: Present scenario and future prospects, Journal of Materials Research. 29 (2014). https://doi.org/10.1557/jmr.2014.189.

[34] I. Yun, Photodiodes - From Fundamentals to Applications, InTech, 2012. https://doi.org/10.5772/3406.

[35] S. Riazimehr, S. Kataria, J.M. Gonzalez-Medina, S. Wagner, M. Shaygan, S. Suckow, F.G. Ruiz, O. Engström, A. Godoy, M.C. Lemme, High Responsivity and Quantum Efficiency of Graphene/Silicon Photodiodes Achieved by Interdigitating Schottky and Gated Regions, ACS Photonics. 6 (2019) 107–115. https://doi.org/10.1021/acsphotonics.8b00951.

[36] S.M. Sze, K.N. Kwok, Physics of Semiconductor Devices, 3rd ed., John Wiley Sons Inc., Hoboken, New Jersey, 2006.

[37] U.Y. Won, B.H. Lee, Y.R. Kim, W.T. Kang, I. Lee, J.E. Kim, Y.H. Lee, W.J. Yu, Efficient photovoltaic effect in graphene/h-BN/silicon heterostructure self-powered photodetector, Nano Research. 14 (2021) 1967–1972. https://doi.org/10.1007/s12274-020-2866-x.

[38] X. Wan, Y. Xu, H. Guo, K. Shehzad, A. Ali, Y. Liu, J. Yang, D. Dai, C. te Lin, L. Liu, H.C. Cheng, F. Wang, X. Wang, H. Lu, W. Hu, X. Pi, Y. Dan, J. Luo, T. Hasan, X. Duan, X. Li, J. Xu, D. Yang, T. Ren, B. Yu, A self-powered high-performance graphene/silicon ultraviolet photodetector with ultra-shallow junction: breaking the limit of silicon?, Npj 2D Materials and Applications. 1 (2017). https://doi.org/10.1038/s41699-017-0008-4.

[39] R. Joly, S. Girod, N. Adjeroud, P. Grysan, J. Polesel-maris, Evidence of negative capacitance and capacitance modulation by light and mechanical stimuli in pt/zno/pt schottky junctions, Sensors. 21 (2021). https://doi.org/10.3390/s21062253.

[40] O. Karaduman, İ. Özkul, C.A. Canbay, Kinetic and structural study on CuAlMnNi shape memory alloy with a novel composition, Advanced Engineering Science. 1 (2021) 13–19. http://publish.mersin.edu.tr/index.php/ades.

[41] C.A. Canbay, O. Karaduman, İ. Özkul, Investigation of varied quenching media effects on the thermodynamical and structural features of a thermally aged CuAlFeMn HTSMA, Physica B: Condensed Matter. 557 (2019) 117–125. https://doi.org/10.1016/j.physb.2019.01.011.

[42] C.A. Canbay, O. Karaduman, İ. Özkul, N. Ünlü, Modifying Thermal and Structural Characteristics of CuAlFeMn Shape Memory Alloy and a Hypothetical Analysis to Optimize Surface-Diffusion Annealing Temperature, Journal of Materials Engineering and Performance. 29 (2020) 7993–8005. https://doi.org/10.1007/s11665-020-05241-7.

[43] O. Karaduman, C.A. Canbay, N. Ünlü, İ. Özkul, Analysis of a newly composed Cu-Al-Mn SMA showing acute SME characteristics, (2019). https://doi.org/10.1063/1.5135437.

[44] C.A. Canbay, O. Karaduman, İ. Özkul, N. Ünlü, Modifying Thermal and Structural Characteristics of CuAlFeMn Shape Memory Alloy and a Hypothetical Analysis to Optimize Surface-Diffusion Annealing Temperature, Journal of Materials Engineering and Performance. 29 (2020) 7993–8005. https://doi.org/10.1007/S11665-020-05241-7.

[45] O. Karaduman, C.A. Canbay, İ. Özkul, S. Aziz Baiz, N. Ünlü, Production and Characterization of Ternary Heusler Shape Memory Alloy with A New Composition, Journal of Materials and Electronic Devices. 1 (2018) 16–19. http://dergi-fytronix.com/index.php/jmed/article/view/24 (accessed November 9, 2021).

[46] C.A. Canbay, O. Karaduman, N. Ünlü, S.A. Baiz, İ. Özkul, Heat treatment and quenching media effects on the thermodynamical, thermoelastical and structural characteristics of a new Cu-based quaternary shape memory alloy, Composites Part B: Engineering. 174 (2019). https://doi.org/10.1016/j.compositesb.2019.106940.

[47] C.A. Canbay, O. Karaduman, N. Ünlü, İ. Özkul, An exploratory research of calorimetric and structural shape memory effect characteristics of Cu–Al–Sn alloy, Physica B: Condensed Matter. 580 (2020). https://doi.org/10.1016/j.physb.2019.411932.

[48] O. Karaduman, C. Aksu Canbay, N. Ünlü, S. Özkul, Structural and thermodynamical study of Cu-Zn-Al shape memory alloys with new compositions produced by hot isostatic press (HIP), in: AIP Conference Proceedings, American Institute of Physics Inc., 2019. https://doi.org/10.1063/1.5135438.

[49] C.A. Canbay, O. Karaduman, N. Ünlü, I. Özkul, Study on Basic Characteristics of CuAlBe Shape Memory Alloy, Brazilian Journal of Physics. 51 (2021) 13–18. https://doi.org/10.1007/s13538-020-00823-1.

[50] O. Karaduman, N. Ünlü, C.A. Canbay, İ. Özkul, S. Aziz Baiz, The Investigation of SME in a Cu-Al-Ni HTSMA, Journal of Materials and Electronic Devices. 1 (2018) 6–10. http://dergi-fytronix.com/index.php/jmed/article/view/22 (accessed October 14, 2021).

[51] C.A. Canbay, O. Karaduman, N. Ünlü, İ. Özkul, M.A. Çiçek, Energetic Behavior Study in Phase Transformations of High Temperature Cu–Al–X (X: Mn, Te, Sn, Hf) Shape Memory Alloys, Transactions of the Indian Institute of Metals. (2021). https://doi.org/10.1007/s12666-021-02241-6.

[52] R.O. Ferreira, L.S. Silva, R.A.G. Silva, Thermal behavior of as-annealed CuAlMnAgZr alloys, Journal of Thermal Analysis and Calorimetry. 146 (2021) 595–600. https://doi.org/10.1007/s10973-020-10002-8.

[53] C.A. Canbay, O. Karaduman, The photo response properties of shape memory alloy thin film based photodiode, Journal of Molecular Structure. 1235 (2021) 130263. https://doi.org/10.1016/j.molstruc.2021.130263.

[54] A. Tataroğlu, F.Z. Pür, The Richardson constant and barrier inhomogeneity at Au/Si 3N4/n-Si (MIS) Schottky diodes, Physica Scripta. 88 (2013). https://doi.org/10.1088/0031-8949/88/01/015801.

[55] V. Balasubramani, J. Chandrasekaran, T.D. Nguyen, S. Maruthamuthu, R. Marnadu, P. Vivek, S. Sugarthi, Colossal photosensitive boost in Schottky diode behaviour with Ce-V2O5 interfaced layer of MIS structure, Sensors and Actuators, A: Physical. 315 (2020). https://doi.org/10.1016/j.sna.2020.112333.

[56] S. Ruzgar, M. Caglar, Fabrication and characterization of solution processed Al/Sn:ZnO/p-Si photodiodes, Materials Science in Semiconductor Processing. 115 (2020) 105076. https://doi.org/10.1016/j.mssp.2020.105076.

[57] A.G. Imer, E. Kaya, A. Dere, A.G. Al-Sehemi, A.A. Al-Ghamdi, A. Karabulut, F. Yakuphanoglu, Illumination impact on the electrical characteristics of Au/Sunset Yellow/n-Si/Au hybrid Schottky diode, Journal of Materials Science: Materials in Electronics. 31 (2020) 14665–14673. https://doi.org/10.1007/s10854-020-04029-8.

[58] P. Vivek, J. Chandrasekaran, R. Marnadu, S. Maruthamuthu, Fabrication of Illumination-Dependent Cu/p-Si Schottky Barrier Diodes by Sandwiching MoO 3 Nanoplates as an Interfacial Layer via JNSP Technique, (n.d.). https://doi.org/10.1007/s11664-020-08137-3.

[59] V. Balasubramani, J. Chandrasekaran, V. Manikandan, T.K. Le, R. Marnadu, P. Vivek, Upgraded photosensitivity under the influence of Yb

doped on V2O5 thin films as an interfacial layer in MIS type Schottky barrier diode as photodiode application, Journal of Solid State Chemistry. 301 (2021). https://doi.org/10.1016/j.jssc.2021.122289.

[60] U.Y. Won, B.H. Lee, Y.R. Kim, W.T. Kang, I. Lee, J.E. Kim, Y.H. Lee, W.J. Yu, Efficient photovoltaic effect in graphene/h-BN/silicon heterostructure self-powered photodetector, Nano Research. 14 (2021) 1967–1972. https://doi.org/10.1007/s12274-020-2866-x.

[61] F. Gul, A simplified method to determine carrier transport mechanisms of metal-oxide resistive random access memory (RRAM) devices, in: Materials Today: Proceedings, Elsevier Ltd, 2021: pp. 6976–6978. https://doi.org/10.1016/j.matpr.2021.03.274.

[62] Z. Çaldiran, M. Şinoforołlu, Ö. Metin, Ş. Aydołan, K. Meral, Space charge limited current mechanism (SCLC) in the graphene oxide-Fe3O4 nanocomposites/n-Si heterojunctions, Journal of Alloys and Compounds. 631 (2015) 261–265. https://doi.org/10.1016/j.jallcom.2015.01.117.

[63] F.C. Chiu, A review on conduction mechanisms in dielectric films, Advances in Materials Science and Engineering. 2014 (2014). https://doi.org/10.1155/2014/578168.